

# Gallium Phosphide Nanowires Grown on SiO<sub>2</sub> by Gas-Source Molecular Beam Epitaxy

Songdan Kang,\* Christian Golz, Carsten Netzel, Irene Mediavilla, Jorge Serrano, Juan Jiménez, and Fariba Hatami



Cite This: *Cryst. Growth Des.* 2023, 23, 2568–2575



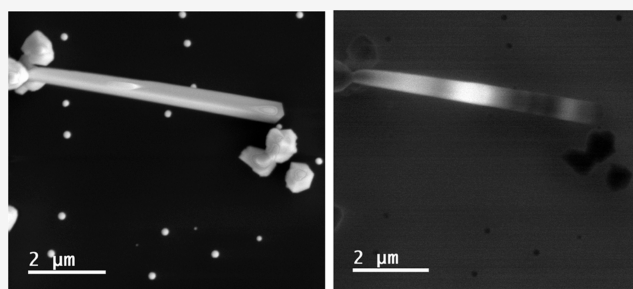
Read Online

ACCESS |

Metrics & More

Article Recommendations

**ABSTRACT:** GaP as one of the III–V semiconductors has an indirect band gap in its natural zinc-blend (ZB) crystal phase, limiting its applications in optoelectronics. The atomic arrangements of the ZB GaP, however, can be changed by adding energy to the system, for example, using strain and defects. In such a way, GaP can be crystallized in the wurtzite (WZ) phase with a direct band gap in the yellow–green range and promising new optical properties. GaP nanostructures offer the great possibility to induce strain, and hence, one can expect to obtain the WZ phase by modifying the geometry and dimensionality of GaP. In this work, we present GaP nanowires (NWs) grown on SiO<sub>2</sub> substrates by gas-source molecular beam epitaxy. Raman measurements on individual GaP NWs indicate that NWs are poly-type crystal structures with the starting growth of the WZ phase, transforming into the ZB phase, and ending as the WZ phase. Photoluminescence at 9 K from an ensemble of NWs shows emissions at 2.09–2.14 eV, which are related to the direct band gap of the WZ phase and peaks between 2.26 and 2.3 eV due to the ZB phase. The emission of the WZ GaP phase is observable up to 160 K. Cathodoluminescence at 83 K shows directly the emission between 2.09 and 2.14 eV along the single NWs, indicating the presence of the WZ phase. Our results demonstrate the realization of poly-type, ZB, and WZ GaP NWs on SiO<sub>2</sub> by gas-source molecular beam epitaxy.



## INTRODUCTION

III–V semiconductor nanowires (NWs) have drawn much attention in areas of next-generation electronics and photonics due to their high carrier mobility,<sup>1,2</sup> tunable electronic structure,<sup>3</sup> and large surface-to-volume ratio,<sup>4,5</sup> enabling them to become promising candidates for optoelectronic devices such as light-emitting devices, solar cells, and photo-detectors.<sup>6,7</sup> Especially, in contrast to relaxed bulk crystals or epilayers, III–V NWs offer a better control to realize either the zincblende (ZB) or the wurtzite (WZ) crystal structures by changing the growth conditions.<sup>8,9</sup> For different crystal structures, a semiconductor will have a different band structure and hence different optical and electric properties. Therefore, by reducing the dimensionality of the semiconductor material into NWs, the electronic structure can be engineered, making possible new and advanced properties and applications. Various methods can be used for the synthesis of III–V NWs including chemical beam epitaxy,<sup>10</sup> pulsed laser ablation,<sup>11</sup> and molecular beam epitaxy (MBE).<sup>12</sup> However, the synthesis faces several challenges, e.g., the narrow growth window and the control of growth direction and the crystal phase. Therefore, elaborated work was carried out for the progress in fabrication of III–V NWs such as GaN,<sup>13</sup> InP,<sup>14,15</sup> and GaAs,<sup>16</sup> exploring their novel properties and promising

applications. WZ InP NWs free of stacking faults and tapering were achieved using selective-area metal–organic vapor-phase epitaxy.<sup>14</sup> These NWs exhibit a high quantum efficiency of about 50%, and room-temperature photonic mode lasing from single NWs shows excellent structural and optical quality. Among III–V semiconductors, GaP has the smallest lattice mismatch with silicon and is a promising material for optical applications due to its high refractive index of 3.37, the band gap in the green range, and high adaptability under harsh weather conditions because of its thermo-optical coefficient and mechanical properties.<sup>17</sup> Moreover, GaP is a promising material for integrated nonlinear photonics. Wilson et al. studied a nonlinear photonics platform with GaP-on-insulator by a direct wafer-bonding approach and investigated integrated waveguides and resonators based on GaP-on-SiO<sub>2</sub> displaying high efficiency in integrated nonlinear photonics.<sup>18</sup> Therefore, the synthesis of GaP on SiO<sub>2</sub> shows remarkable potential for

**Received:** December 6, 2022

**Revised:** March 1, 2023

**Published:** March 10, 2023



optoelectronic devices. However, the indirect band gap of GaP in the ZB crystal structure severely limits its applications, particularly as a light emitter. Nevertheless, band structure calculations<sup>19,20</sup> predicted that GaP under pressure or when grown as NWs can have a WZ structure with a direct band gap. De et al. calculated the energy of the direct band gap for WZ GaP to be 2.251 eV (9v to 8c).<sup>19</sup> Belabbes et al. did the calculations for the cubic 3C phase with a band gap energy of 2.33 eV from  $\Gamma$ -X and a direct transition energy of 2.79 eV from  $\Gamma$ - $\Gamma$  and a hexagonal 2H phase with a direct band gap of 2.181 eV from  $\Gamma$ - $\Gamma$  and an indirect transition energy of 2.266 eV from  $\Gamma$ -M.<sup>20</sup> Therefore, the fabrication and investigation of WZ GaP have attracted a great deal of attention, and the theoretical predictions have been verified by several experimental results. Assali et al. reported the fabrication of GaP NWs with a pure WZ crystal structure and demonstrated the direct nature of the band gap, which yields light emission at 2.086 eV.<sup>21</sup> Silva et al. proved the pseudo-direct band gap of WZ GaP grown by the NW-crawling-assisted vapor-liquid-solid method, and their result showed a 10 K band gap at 2.19 eV.<sup>22</sup> The electronic band gap of wurtzite GaP in experimental and theoretical studies shows different values; hence, more work and investigation on this are needed.

In this work, self-catalyzed GaP NWs were grown on SiO<sub>2</sub> using gas-source MBE (GS-MBE). The nucleation of the NWs occurs via a vapor-liquid-solid mechanism. The morphology of the samples was investigated using scanning electron microscopy (SEM). The structural and optical properties were characterized using micro-Raman spectroscopy, photoluminescence (PL), and cathodoluminescence (CL). Our results show that the GaP NWs grown on SiO<sub>2</sub> are a mixed ensemble of the polytype WZ/ZB/WZ, pure ZB, and WZ NWs.

## EXPERIMENTAL SECTION

GaP NWs were grown on SiO<sub>2</sub> substrates in a Riber 32 molecular beam epitaxy system, using thermally cracked phosphine (PH<sub>3</sub>) as gas source and solid gallium (Ga) source. The oxide layer on the Si substrate was deposited using tetraethylorthosilicate in plasma-enhanced chemical vapor deposition. After loading into the growth chamber of the MBE system, the substrate was heated at 720 °C for 5 min to desorb the contamination from the surface and make it ready for the growth of GaP. Afterward, the temperature was reduced to a growth temperature of 646 °C. Then, the growth was initiated by simultaneously introducing Ga and PH<sub>3</sub> flux of 2.5 sccm. Under the same condition, the growth rate for planar GaP is 1 Å/s. The morphology was observed with a SEM system (SEM-Pioneer two, Raith Fabrication). Raman spectra were measured with a Horiba LabRAM Soleil Raman spectrometer, with a Symphony charge-coupled device detector. A solid-state laser ( $\lambda = 532$  nm) was used as the exciting source with a power of 1 mW and an approximate irradiance of  $100 \text{ kW} \times \text{cm}^{-2}$ , and the spot diameter of the Raman beam was about 1  $\mu\text{m}$ . Acquisition time was set at 3 s and the spectral split aperture at 200  $\mu\text{m}$  and grating at 2400 g/mm, obtaining a spectral resolution better than 1  $\text{cm}^{-1}$ . PL was measured with excitation from an argon ion laser ( $\lambda = 458$  nm,  $P = 100 \text{ W}/\text{cm}^2$ ) or a HeCd laser ( $\lambda = 325$  nm,  $P = 250 \text{ W}/\text{cm}^2$ ) between 10 and 300 K. CL was measured at  $T = 83$  K in a Zeiss Ultra scanning electron microscope with a MONOCL4 detection unit from Gatan. The electron beam width was approximately 1 nm, and an acceleration voltage of 7 kV and a beam current of 970 pA were used.

## RESULTS AND DISCUSSION

Figure 1 is the plan-view SEM image of a sample after 2 h growth of GaP. The randomly distributed nanocrystals on the

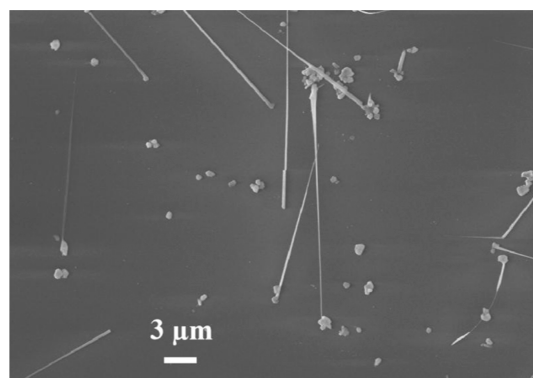


**Figure 1.** Plan-view SEM image of GaP NWs grown on SiO<sub>2</sub>. The randomly distributed particles are GaP crystals which act as pedestals for growth of GaP NWs.

SiO<sub>2</sub> surface are GaP particles. These nanocrystals are the pedestals for growth of NWs. The nucleation of the NWs occurs via the vapor-liquid-solid mechanism with a Ga droplet. The growth and mechanisms of self-catalyzed GaP NWs by droplet consumption have been investigated elaborately.<sup>23</sup> In our case, the droplets are completely consumed. The end of NWs is shaped like a sharp needle. NWs with a length of up to 20  $\mu\text{m}$  are distributed irregularly with large spacings between them. The low density of GaP structures allows the investigation of individual NWs without any additional preparation or transferring of the wires to a foreign substrate. Hence, it is certain that no part of the wires is missing, or no defects due to the preparation are induced. Furthermore, any kind of opto-electronic coupling between the NWs is excluded. Here, we focus on Raman and optical characteristics of representative individual GaP NWs.

It is reported that the Raman spectrum of WZ GaP exhibits peaks at 78.1  $\text{cm}^{-1}$  (EL 2 mode), 355.8  $\text{cm}^{-1}$  (EH 2 mode), 363.4  $\text{cm}^{-1}$  [ $A_1$  (transverse optical, TO)/ $E_1$  (TO) phonon mode], 395.7  $\text{cm}^{-1}$  [ $A_1$  (longitudinal optical, LO) mode], and 401.4  $\text{cm}^{-1}$  [ $E_1$  (LO) mode].<sup>22</sup> The Raman spectrum of ZB GaP NWs has been reported with peaks at 365  $\text{cm}^{-1}$  (TO), 385  $\text{cm}^{-1}$  (surface optical, SO, phonon mode), and 401  $\text{cm}^{-1}$  (LO)<sup>24</sup> (bulk ZB GaP:<sup>25</sup> TO at 367  $\text{cm}^{-1}$  and LO at 403  $\text{cm}^{-1}$ ). EL 2 and EH 2 nonpolar phonon modes are featured WZ modes compared with phonon modes of the ZB phase. One can scan a single NW to identify the structural information and phase purity. To this propose,  $\mu$ -Raman measurements using the 532 nm laser and a power of 0.57 mW were performed on different segments of several single NWs. Figure 2a displays Raman spectra along a representative GaP NW with a length of 7  $\mu\text{m}$ . The inset in Figure 2a shows the optical image of this NW. According to the Raman spectra, the EL 2 and EH 2 modes (78.1 and 355.8  $\text{cm}^{-1}$ , respectively), associated with the WZ phase, appear at the beginning and the end of the NW. At the interface between WZ and ZB, one observes a downshift of the TO mode, which is likely due to the slight lattice distortion induced by strain or the consequence of the mixed modes (WZ + ZB) probed by Raman at the interface. The data indicate that the lower part of the NW is in the WZ phase, transforming later into the ZB phase, and finally ending the growth in the WZ phase. Figure 2b is a typical Raman spectrum of WZ GaP, taken from the bottom of the NW. Figure 2c,d are magnifications of the spectrum in the wavenumber range below 100  $\text{cm}^{-1}$  and the

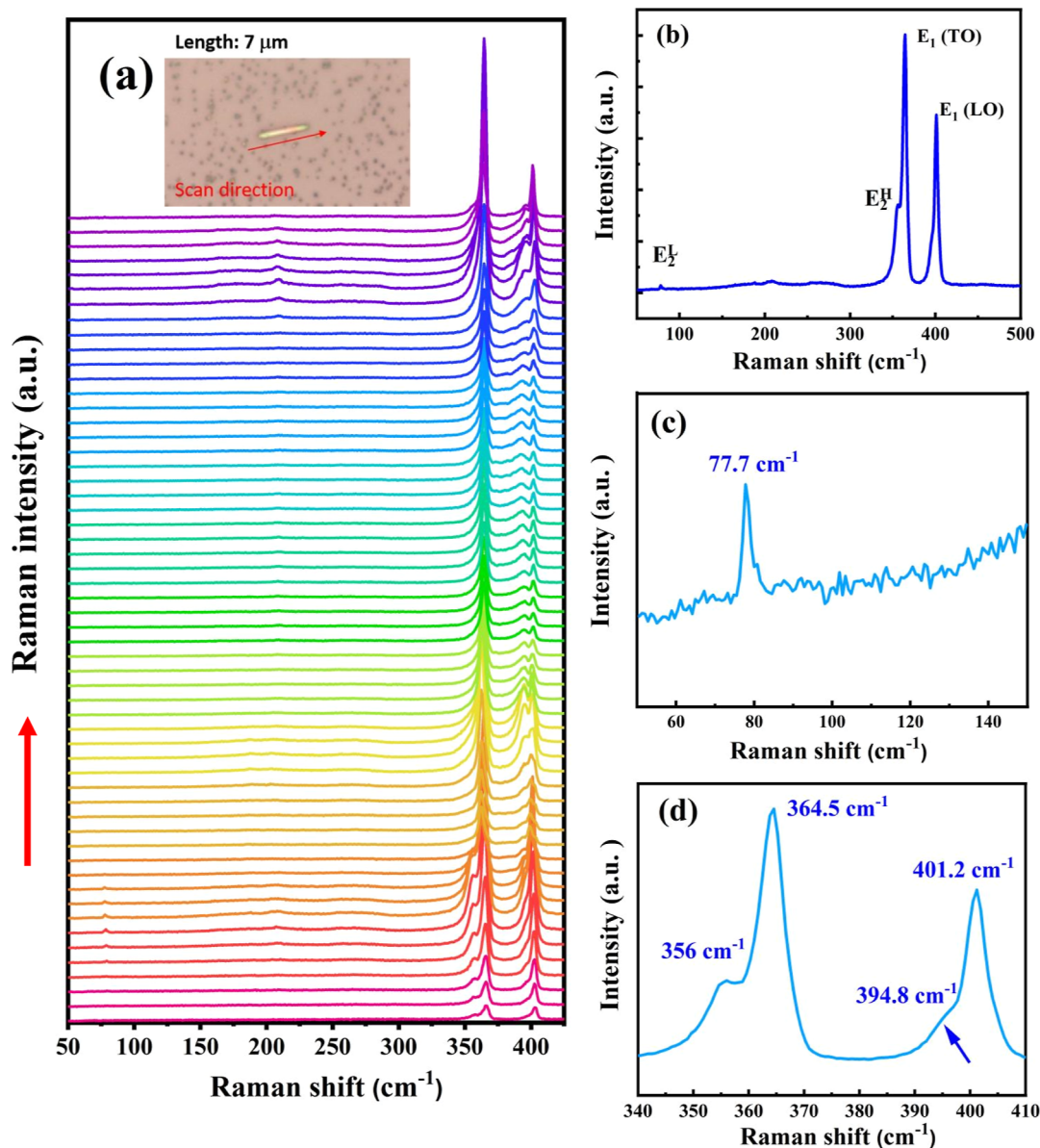


**Figure 2.** (a) Raman spectra along a 7  $\mu\text{m}$  NW. The optical image is shown in the inset. (b) Typical Raman spectrum of the WZ phase of GaP. (c) Zoom-in of the Raman spectrum in the range of 50–150  $\text{cm}^{-1}$ . (d) Zoom-in of the Raman spectrum in the range of 340–410  $\text{cm}^{-1}$ .

**Table 1.** Summarization of Raman Shifts of WZ and ZB GaP

		Raman shifts (phonon modes)				references
WZ GaP	78.1 $\text{cm}^{-1}$ (EL 2)	355.8 $\text{cm}^{-1}$ (EH 2)	363.4 $\text{cm}^{-1}$ [A <sub>1</sub> (TO)]/E <sub>1</sub> (TO)]	395.7 $\text{cm}^{-1}$ [A <sub>1</sub> (LO)]	401.4 $\text{cm}^{-1}$ [E <sub>1</sub> (LO)]	22
ZB GaP NWs			365 $\text{cm}^{-1}$ (TO)	385 $\text{cm}^{-1}$ (SO)	401 $\text{cm}^{-1}$ (LO)	24
bulk ZB GaP			367 $\text{cm}^{-1}$ (TO)		403 $\text{cm}^{-1}$ (LO)	25
WZ phase of the NW	77.7 $\text{cm}^{-1}$ (EL 2)	356 $\text{cm}^{-1}$ (EH 2)	364.5 $\text{cm}^{-1}$ [E <sub>1</sub> (TO)]	394.8 $\text{cm}^{-1}$ [A <sub>1</sub> (LO)]	401.2 $\text{cm}^{-1}$ [E <sub>1</sub> (LO)]	this work
ZB phase of the NW			363 $\text{cm}^{-1}$ (TO)	394 $\text{cm}^{-1}$ (SO)	401 $\text{cm}^{-1}$ (LO)	this work

range between 340 and 410  $\text{cm}^{-1}$ , respectively. The WZ phonons modes at 77.7  $\text{cm}^{-1}$  (EL 2), 356  $\text{cm}^{-1}$  (EH 2), 364.5  $\text{cm}^{-1}$  [E<sub>1</sub> (TO)], 394.8  $\text{cm}^{-1}$  [A<sub>1</sub> (LO)], and 401.2  $\text{cm}^{-1}$  [E<sub>1</sub> (LO)] are unambiguously identified. In the middle segment of the NW, the 363  $\text{cm}^{-1}$  (TO), 394  $\text{cm}^{-1}$  (SO), and 401  $\text{cm}^{-1}$  (LO) phonon modes of the ZB phase are observed. Raman

shifts of WZ and ZB GaP from literature studies and this work are summarized in Table 1.

The Raman spectra along another GaP NW with a length of 11  $\mu\text{m}$  are shown in Figure 3a. The WZ phase appears at the bottom and the end of the NW, as identified by the Raman mode at 77.7  $\text{cm}^{-1}$ , in a similar way to that observed for the NW of Figure 2. Figure 3b presents the Raman spectra in the

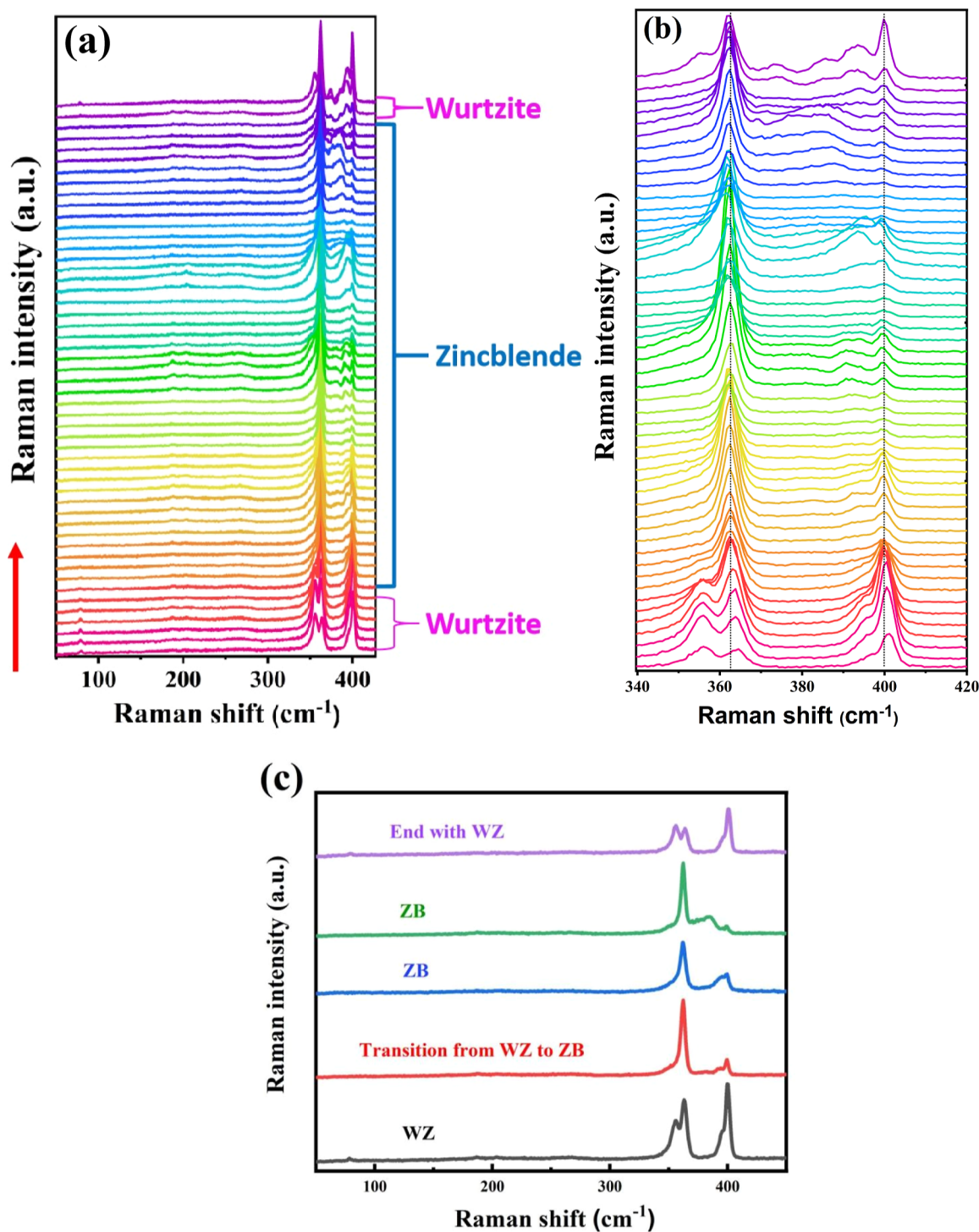


**Figure 3.** (a) Raman spectra along a 11  $\mu\text{m}$  NW. (b) Close-up of these spectra in the range of 340–420  $\text{cm}^{-1}$ . (c) Raman spectra from five segments of a single NW from bottom to top.

340–420  $\text{cm}^{-1}$  spectral range. In order to follow the change in the phonon characteristics along the NWs and hence the change in the crystal phase, five selected Raman spectra are displayed in Figure 3c. The longitudinal optical phonon in ZB GaP is symmetry-forbidden for Raman back-scattering from the (110) plane. Therefore, the middle section of the NW, which is the ZB phase, shows a main TO mode, as the face exposed to the laser beam is (110), and a weak LO Raman peak, a consequence of the deviation from the true backscattering on (110), because of the NW shape and the

numerical aperture of the objective. The phonon mode at about 385  $\text{cm}^{-1}$  between TO and LO phonons for ZB GaP is attributed to a surface phonon (SO), which is absent in the WZ phase. The SO mode depends on the surface, the diameter, and the surrounding medium.<sup>26</sup> At the WZ phase, the forbidden LO mode is present because of the relaxation of the selection rule for the WZ phase. This mode shows significantly high intensity which is even higher than that of the TO mode, most likely caused by resonance effects.<sup>22</sup> Raman measurement on individual NWs proves that WZ/ZB and ZB/

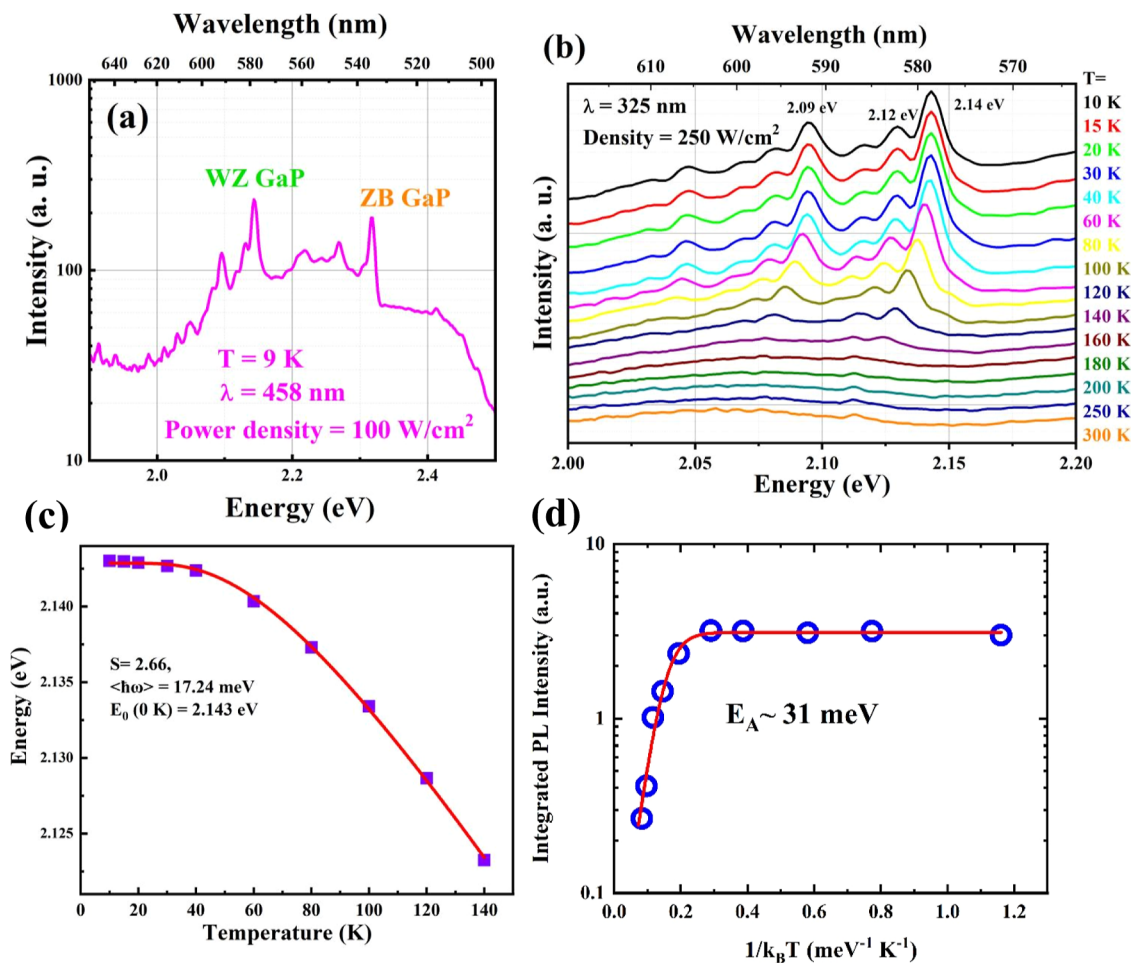


**Figure 4.** (a) PL spectrum at 9 K. (b) Temperature-dependent PL spectra. A blue shift and quenching can be observed at the emission energy of 2.14 eV with the increasing temperature. (c) Temperature dependence of exciton-bound related emission energy (2.14 eV peak) and the corresponding curve fitted with eq 1.  $S$  corresponds to the strength of electron–phonon coupling, and  $\langle \hbar\omega \rangle$  is average phonon energy. (d) Integrated PL intensity of the emission peak at 2.14 eV as a function of  $1/k_B T$  and the fitting curve according to the Arrhenius equation.  $E_A$  is the activation energy for thermal dissociation of the bound excitons.

WZ transformations occur along the GaP NWs. The Raman results are a clear indicator of the existence of the WZ phase in the single GaP NWs.

For exploring the optical emission of the GaP NWs, PL and CL measurements were carried out. Figure 4a shows the PL spectrum of an ensemble of GaP NWs on the SiO<sub>2</sub> substrate, measured at 9 K and excited by a 458 nm laser with a power density of 100 W/cm<sup>2</sup> (spot size approximately 70 μm in diameter). The spectrum contains several peaks between 2.09 and 2.31 eV and broad emission features in the energy range between 2.1 and 2.5 eV. The calculated direct band gap of WZ GaP is related to  $\Gamma_{9v}-\Gamma_{8c}$  transition at 2.123 eV, which is weakly allowed, while transitions  $\Gamma_{7v+}-\Gamma_{8c}$  with an energy of 2.166 eV and  $\Gamma_{7v-}-\Gamma_{8c}$  with an energy of 2.298 eV are forbidden.<sup>27</sup> Trap-bound excitons relax the selection rules for optical transitions that cause an increase in the transition probability and can explain the observed peak at 2.14 eV. The emission energy of this peak  $E_{PL}$  is related directly to  $E_g$  and the WZ band gap ( $\Gamma_{9v}-\Gamma_{8c}$ ) energy,  $E_{PL} = E_g - \Delta E$ , where  $\Delta E$  is the sum of the free exciton energy and the binding energy of the free excitons to the trap centers.<sup>28</sup> In the present work, we observe further sharp emission lines between 2.02 and 2.13 eV which are a set of acoustical and optical phonon replicas of the 2.14 eV transition.<sup>27</sup> Donor-acceptor-pair (DAP) transitions in

WZ GaP may contribute to the intensity background between 2.0 and 2.15 eV in our PL measurements but are not resolved under the high-excitation conditions. The peak at 2.26 eV could be a feature from WZ GaP and be identified with the bound exciton  $\chi$  transition;<sup>27</sup> however, similar emission has been reported for the ZB GaP, and therefore, the emission can be related to the excitons bound to the neutral donor/acceptor in ZB GaP.<sup>29</sup> The peak at 2.31 eV is, on the other hand, a direct observation for the indirect band gap from  $\Gamma$  to X minimum at 9 K ZB GaP, showing that the ZB GaP phase is definitely present in the ensemble of nanostructures too. The broad intensity background between 2.1 and 2.5 eV may stem from the SiO<sub>2</sub> substrate.<sup>30</sup> Assali et al.<sup>27</sup> did the optical investigation on WZ GaP NWs at 4 K and reported similar emission lines. They attributed peaks at 2.115 and 2.088 eV to the donor–acceptor pair recombination and the sharp lines at 2.140, 2.164, and 2.252 eV to bound excitons in WZ GaP, from which a band gap of 2.190 eV is obtained. A Burstein–Moss band-filling continuum between 2.180 and 2.253 eV was observed.

In order to further investigate the origin of the emission lines, PL measurements in the temperature range between 10 and 300 K were performed. The sample was excited with a laser of 325 nm and an excitation density of 250 W/cm<sup>2</sup>. As it

can be seen in Figure 4b, with increasing temperatures in the range of 10–160 K, a red shift, broadening, and quenching of the peak related to the WZ GaP happen. According to the temperature-dependent band gap equation due to electron–phonon coupling (eq 1) developed by O’Donnell and Chen,<sup>31</sup> with increasing temperature, the lattice phonons are excited in larger numbers, leading to change of the chemical bonding due to electron–phonon interaction and hence narrowing of the band gap.<sup>31</sup> Equation 1 describes this model

$$E_g(T) = E_0 - S\langle\hbar\omega\rangle(\cot h(\langle\hbar\omega\rangle/2k_{\text{BT}}) - 1) \quad (1)$$

where  $E_g(T)$  is the bandgap at temperature  $T$ ,  $S$  is a dimensionless material constant which is a measure of strength of electron–phonon coupling,  $k_{\text{B}}$  is the Boltzmann constant, and  $\langle\hbar\omega\rangle$  is average phonon energy. Since the binding energy of excitons and the trap energy are not temperature-dependent, we can use this model (eq 1) to fit the temperature dependence of the PL peak at 2.14 eV. The measured data and the corresponding fit are shown in Figure 4c. The equation leads to an excellent fit with values of  $S = 2.66$ ,  $\langle\hbar\omega\rangle = 17.24$  meV, and  $E_0 = 2.143$  eV. We could not find any reported values for WZ GaP, but the obtained values for strength of electron–phonon coupling and the average phonon energy for the WZ GaP are lower than the reported values for ZB GaP ( $S = 3.35$ ,  $\langle\hbar\omega\rangle = 43.6$  meV<sup>31</sup>). Note that the value of 2.143 eV is lower than the band gap energy due to the energy shift  $\Delta E$  related to the trap-bound excitons ( $E_g = E_{\text{PL}} + \Delta E$ ).

In order to estimate the band gap energy, we first need to know the exciton binding energy, which contains the free exciton energy and the binding energy of the free excitons to the trap centers. The exciton binding energy can be investigated by temperature dependence of the light output associated with the trap-bound exciton system, ( $T, X$ ). The main processes for the thermal dissociation of the ( $T, X$ ) system and hence decrease of the radiative recombination are (I) either when the dissociation results in a free exciton because the binding energy of the exciton to the trap center is overcome, (II) or the ( $T, X$ ) system dissociates, resulting in a free electron and a free hole. For the first case, the activation energy displays the binding energy of the free excitons to the trap center. For process (II), the exciton binding energy  $\Delta E$  is the activation energy, including both the free exciton energy and the binding energy of the free excitons to the trap centers. Therefore, we apply the Arrhenius model to estimate the activation energy.<sup>32</sup> The integrated PL intensity of the energy peak at 2.14 eV as a function of temperature can be described by

$$I = \frac{I_0}{1 + A \exp(-E_a/k_{\text{B}}T)} \quad (2)$$

where  $A$  is the non-radiative recombination process coefficient,  $k_{\text{B}}$  is again the Boltzmann constant, and  $E_a$  is the activation energy for thermal dissociation of the bound excitons.<sup>32</sup> Figure 4d shows the integrated PL intensity as a function of  $1/k_{\text{B}}T$  and the fitting curve using the Arrhenius equation, which results in a thermal activation energy of  $31 \pm 3$  meV for trap-bound excitons in WZ GaP NWs. This value is higher than the calculated free exciton energy of about 17 meV,<sup>27</sup> and we approximately considered it the exciton binding energy, leading to an estimated band gap energy of about  $2.174 \pm 0.003$  eV at 0 K.

In order to study the light emission from different segments of a single NW and hence gain knowledge on electronic structures and crystal phases along the NW, spatially resolved CL spectra recorded along several single GaP NWs were analyzed. Figure 5a is a SEM image of one GaP NW with a

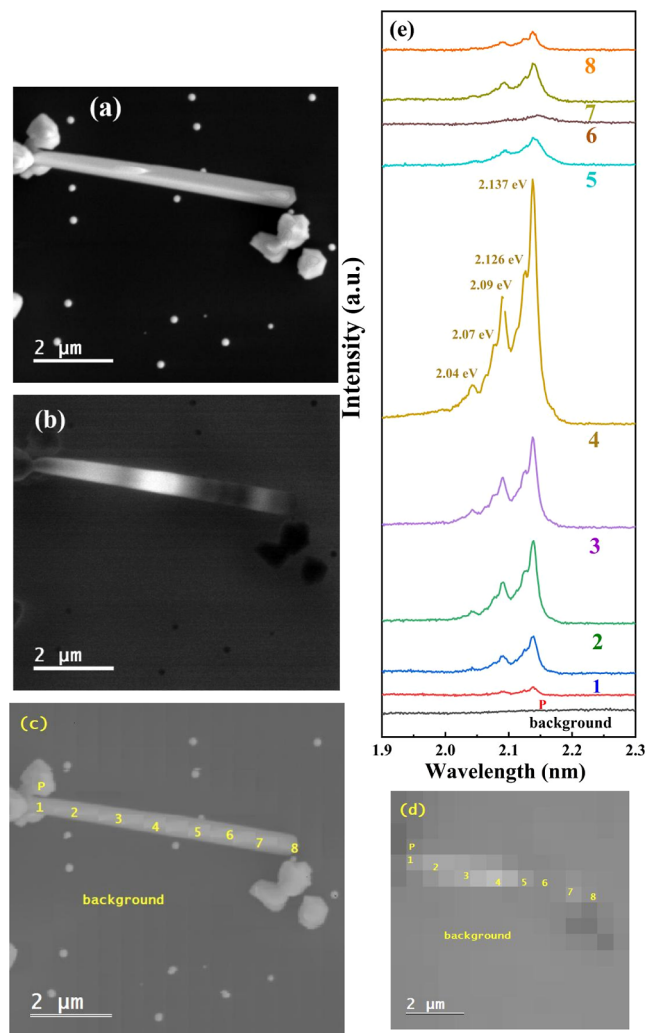


**Figure 5.** (a) Scanning electron image of an individual GaP NW. (b) Panchromatic CL image of the same area, which reflects the emission intensity. The NW has the highest intensity in the middle section, while the substrate has no emission. (c) Signal image. (d) Spectral mapping. (e) CL spectra at 83 K along the NW as indicated in (a,b).

projected length of  $6.5 \mu\text{m}$  and a base diameter of  $420$  nm. The corresponding panchromatic CL image is shown in Figure 5b revealing the CL intensity distribution on the SEM image area. The  $\text{SiO}_2$  substrate shows nearly zero intensity, while the GaP pedestal exhibits a weak emission, and the NW presents a high emission intensity reaching the highest brightness in its middle section. Figure 5c is the signal image, and Figure 5d shows the corresponding spectrum mapping which is able to get each spectrum from the interesting area of the image; therefore, with mapping, the emission from the pedestal and segments of NWs can be distinguished. Figure 5e shows CL spectra at 83 K along the NW from the base to the top. The  $\text{SiO}_2$  substrate has no emission, while the pedestal has a weak emission at 2.137 and 2.09 eV which indicates the WZ phase for the pedestal. The emissions from the NW have the highest intensity in the

middle part. All segments of the NW show a peak at 2.137 eV which is related to the bound excitonic recombination in the WZ GaP. The highest intensity within the NW analyzed in Figure 5 was seen in segment 4, which has CL emission at the energies of 2.137, 2.126, 2.09, 2.07, and 2.04 eV as indicated in Figure 5c. Another peak at 2.09 eV is attributed to DAP recombination and appears in the PL spectra as shown in Figure 4a as well. Peaks at 2.12, 2.07, and 2.04 eV may originate from phonon replicas. The absence of the emission from the ZB phase in this NW may indicate the pure WZ phase. However, we do not expect any emission from indirect-band gap ZB GaP at 83 K, and therefore, the wire may contain small segments of the ZB phase as well and be a polytype structure. On the other hand, some NWs do not emit any CL signal at 83 K, which obviously verifies the ZB structure of those NWs. Hence, CL results indicate that GaP NWs crystallize either in the pure ZB phase or in WZ structures which may hold small ZB segments. The CL spectrum is similar to the PL spectrum at 83 K. The sharp emission at 2.137 eV is exactly the value obtained from PL and is attributed to the trap-bound excitons of the WZ structure. With the estimated exciton binding energy of  $31 \pm 3$  meV using the Arrhenius equation, the band gap energy of WZ GaP at 83 K is  $2.168 \pm 0.003$  eV. Table 2 summarizes the band gap

**Table 2. Band Gap Energy of WZ GaP from Previous Studies and This Work**

WZ band gap energy	references
2.25 eV (theory prediction, empirical pseudopotential)	De <sup>19</sup> and Pryor
2.181 eV (theory prediction for H <sub>2</sub> , LDA-1/2)	Belabbes <sup>20</sup> et al.
2.2 eV (10 K) PL, NWs	Maliakkal <sup>33</sup> et al.
2.190 eV (4 K) PL, NWs	Assali <sup>27</sup> et al.
2.19 eV (10 K) absorption, volume GaP	Silva <sup>22</sup> et al.
2.13 eV (10 K) PL, NWs	Halder <sup>34</sup> et al.
2.171 ± 0.003 eV (10 K)	this work
2.168 ± 0.003 eV (83 K) CL, PL	this work

energy of WZ GaP from theoretical predictions and experimental measurements. Our results are in the same range and very close to the measured absorption edge of pure volume WZ GaP.<sup>33</sup>

## CONCLUSIONS

In summary, GaP NWs were successfully grown on SiO<sub>2</sub> substrates by GS-MBE. The structural and electronic properties of individual NWs were studied via Raman, PL, and CL measurements. The WZ GaP has unique Raman modes: the EL 2 mode and EH 2 mode in contrast to the ZB phase. The Raman study on individual NWs showed that one type of NW is WZ-base/ZB main-body/WZ-end. PL measurements verify the Raman results. The luminescence emission at about 2.14 eV at 9 K is due to the bound excitonic recombination in the WZ GaP. The emission due to the WZ GaP phase can be measured up to 160 K, whereas the emission due to the ZB phase disappears for temperatures higher than 30 K. The analysis of the PL temperature dependence of the bound excitons results in an exciton binding energy of  $31 \pm 3$  meV for the WZ phase. Using CL measurements at 83 K, we characterized single GaP NWs with dominant emission at 2.137 eV, indicating the WZ phase. Several NWs do not show any CL signal at 83 K, which is a clear indication of their pure ZB structure. At 10 K, the estimated direct band gap energy for

the WZ phase is about 2.171 eV, and the indirect band gap energy of the ZB phase is about 2.31 eV. The results presented herein reveal that GaP NWs on SiO<sub>2</sub> are a mixed arrangement of the ZB, WZ, and polytype phases, giving a high versatility for the nanodevices based on GaP NWs on SiO<sub>2</sub>.

## AUTHOR INFORMATION

### Corresponding Author

**Songdan Kang** – Institut für Physik, Mathematisch-Naturwissenschaftliche Fakultät, Humboldt Universität zu Berlin, 12489 Berlin, Germany; [orcid.org/0000-0002-0645-1123](https://orcid.org/0000-0002-0645-1123); Email: [skang@physik.hu-berlin.de](mailto:skang@physik.hu-berlin.de)

### Authors

**Christian Golz** – Institut für Physik, Mathematisch-Naturwissenschaftliche Fakultät, Humboldt Universität zu Berlin, 12489 Berlin, Germany

**Carsten Netzel** – Ferdinand-Braun-Institut (FBH), 12489 Berlin, Germany

**Irene Mediavilla** – GdS-Optronlab Group, Department Física de la Materia Condensada, Cristalografía y Mineralogía, Universidad de Valladolid, 47011 Valladolid, Spain

**Jorge Serrano** – GdS-Optronlab Group, Department Física de la Materia Condensada, Cristalografía y Mineralogía, Universidad de Valladolid, 47011 Valladolid, Spain

**Juan Jiménez** – GdS-Optronlab Group, Department Física de la Materia Condensada, Cristalografía y Mineralogía, Universidad de Valladolid, 47011 Valladolid, Spain

**Fariba Hatami** – Institut für Physik, Mathematisch-Naturwissenschaftliche Fakultät, Humboldt Universität zu Berlin, 12489 Berlin, Germany

Complete contact information is available at: <https://pubs.acs.org/10.1021/acs.cgd.2c01447>

### Author Contributions

The manuscript was written through contributions of all authors. All authors have given approval to the final version of the manuscript.

### Notes

The authors declare no competing financial interest.

## ACKNOWLEDGMENTS

S.K. thanks the China Scholarship Council for her research grant. The authors thank O. Skibitzki for providing the wafer. This work was supported by the German Research Foundation (DFG grant no: 428250328). I.M., J.S., and J.J. were funded by Spanish Agencia Estatal de Investigación (project: PID2021-126046OB-C22).

## REFERENCES

- (1) Badawy, G.; Gazibegovic, S.; Borsoi, F.; Heedt, S.; Wang, C.-A.; Koelling, S.; Verheijen, M. A.; Kouwenhoven, L. P.; Bakkers, E. P. A. M. High Mobility Stemless InSb Nanowires. *Nano Lett.* **2019**, *19*, 3575–3582.
- (2) Ford, A. C.; Chuang, S.; Ho, J. C.; Chueh, Y. L.; Fan, Z.; Javey, A. Patterned p-Doping of InAs Nanowires by Gas-Phase Surface Diffusion of Zn. *Nano Lett.* **2010**, *10*, 509–513.
- (3) Ba Hoang, T. B.; Moses, A. F.; Ahtapodov, L.; Zhou, H.; Dheeraj, D. L.; van Helvoort, A. T. J.; Fimland, B. O.; Weman, H. Engineering Parallel and Perpendicular Polarized Photoluminescence From a Single Semiconductor Nanowire by Crystal Phase Control. *Nano Lett.* **2010**, *10*, 2927–2933.
- (4) Liu, C.; Dasgupta, N. P.; Yang, P. Semiconductor Nanowires for Artificial Photosynthesis. *Chem. Mater.* **2014**, *26*, 415–422.

- (5) Walter, M. G.; Warren, E. L.; McKone, J. R.; Boettcher, S. W.; Mi, Q.; Santori, E. A.; Lewis, N. S. Solar Water Splitting Cells. *Chem. Rev.* **2010**, *110*, 6446–6473.
- (6) Fang, M.; Han, N.; Wang, F.; Yang, Z.; Yip, S.; Dong, G.; Hou, J. J.; Chueh, Y.; Ho, J. C. III–V Nanowires: Synthesis, Property Manipulations, and Device Applications. *J. Nanomater.* **2014**, *2014*, 14.
- (7) Barrigón, E.; Heurlin, M.; Bi, Z.; Monemar, B.; Samuelson, L. Synthesis and Applications of III–V Nanowires. *Chem. Rev.* **2019**, *119*, 9170–9220.
- (8) Joyce, H. J.; Wong-Leung, J. W.; Gao, Q.; Tan, H. H.; Jagadish, C. Phase Perfection in Zinc Blende and Wurtzite III–V Nanowires Using Basic Growth Parameters. *Nano Lett.* **2010**, *10*, 908–915.
- (9) Dick, K. A.; Caroff, P.; Bolinsson, J.; Messing, M. E.; Johansson, J.; Deppert, K.; Wallenberg, L. R.; Samuelson, L. Control of III–V Nanowire Crystal Structure by Growth Parameter Tuning. *Semicond. Sci. Technol.* **2010**, *25*, 024009.
- (10) Persson, A. I.; Larsson, M. W.; Stenström, S.; Ohlsson, B. J.; Samuelson, L.; Wallenberg, L. R. Solid-Phase Diffusion Mechanism for GaAs Nanowire Growth. *Nat. Mater.* **2004**, *3*, 677–681.
- (11) Morales, A. M.; Lieber, C. M. A Laser Ablation Method for the Synthesis Crystalline Semiconductor Nanowires. *Science* **1998**, *279*, 208–211.
- (12) Colombo, C.; Spirkoska, D.; Frimmer, M.; Abstreiter, G.; Fontcuberta i Morral, A. F. I. Ga-Assisted Catalyst-Free Growth Mechanism of GaAs Nanowires by Molecular Beam Epitaxy. *Phys. Rev. B: Condens. Matter Mater. Phys.* **2008**, *77*, 155326.
- (13) Fernández-Garrido, S.; Auzelle, T.; Lähnemann, J.; Wimmer, K.; Tahraouia, A.; Brandt, O. Top-Down Fabrication of Ordered Arrays of GaN Nanowires by Selective Area Sublimation. *Nanoscale Adv.* **2019**, *1*, 1893–1900.
- (14) Avit, G.; Lekhal, K.; Andre, Y.; Bougerol, C.; Reveret, F.; Leymarie, J.; Gil, E.; Monier, G.; Castelluci, D.; Trassoudaine, A. Selective-Area Epitaxy of Pure Wurtzite InP Nanowires: High Quantum Efficiency and Room-Temperature Lasing. *Nano Lett.* **2014**, *14*, 5206–5211.
- (15) Krishnamachari, U.; Borgstrom, M.; Ohlsson, B. J.; Panev, N.; Samuelson, L.; Seifert, W.; Larsson, M. W.; Wallenberg, L. R. Defect-Free InP Nanowires Grown in (001) Direction on InP (001). *Appl. Phys. Lett.* **2004**, *85*, 2077.
- (16) Jansen, M. M.; Perla, P.; Kaladzian, M.; von den Driesch, N.; Janßen, J.; Luysberg, M.; Lepsa, M. I.; Grützmacher, D.; Pawlis, A. Phase-Pure Wurtzite GaAs Nanowires Grown by Self-Catalyzed Selective Area Molecular Beam Epitaxy for Advanced Laser Devices and Quantum Disks. *ACS Appl. Nano Mater.* **2020**, *3*, 11037–11047.
- (17) Choi, W.; Huang, H. C.; Fan, S.; Mohseni, P. K.; Lee, M. L.; Li, X. Selective Area Heteroepitaxy of p-i-n Junction GaP Nanopillar Arrays on Si (111) by MOCVD. *J. Quant. Electron.* **2022**, *58*, 1–6.
- (18) Wilson, D. J.; Schneider, K.; Hönl, S.; Anderson, M.; Baumgartner, Y.; Czornomaz, L.; Kippenberg, T. J.; Seidler, P. Integrated Gallium Phosphide Nonlinear Photonics. *Nat. Photonics* **2020**, *14*, 57–62.
- (19) De, A.; Pryor, C. E. Predicted Band Structures of III-V Semiconductors in the Wurtzite Phase. *Phys. Rev. B: Condens. Matter Mater. Phys.* **2010**, *81*, 155210.
- (20) Belabbes, A.; Panse, C.; Furthmüller, J.; Bechstedt, F. Electronic Bands of III-V Semiconductor Polytypes and Their Alignment. *Phys. Rev. B: Condens. Matter Mater. Phys.* **2012**, *86*, 075208.
- (21) Assali, S.; Zardo, I.; Plissard, S.; Kriegner, D.; Verheijen, M. A.; Bauer, G.; Meijerink, A.; Belabbes, A.; Bechstedt, F.; Haverkort, J. E. M.; Bakkers, E. P. A. M. Direct Band Gap Wurtzite Gallium Phosphide Nanowires. *Nano Lett.* **2013**, *13*, 1559–1563.
- (22) Silva, B. C.; Couto, O. D. D., Jr.; Obata, H. T.; Lima, M. M.; Bonani, F. D.; Oliveira, C. E.; Sipahi, G. M.; Iikawa, F.; Cotta, M. A. Optical Absorption Exhibits Pseudo-Direct Band Gap of Wurtzite Gallium Phosphide. *Sci. Rep.* **2020**, *10*, 7904.
- (23) Fedorov, V. V.; Dvoretckaja, L. N.; Kirilenko, D. A.; Mukhin, I. S.; Dubrovskii, V. G. Formation of Wurtzite Sections in Self-Catalyzed GaP Nanowires by Droplet Consumption. *Nanotechnology* **2021**, *32*, 495601.
- (24) Gupta, R.; Xiong, Q.; Mahan, G. D.; Eklund, P. C. Surface Optical Phonons in Gallium Phosphide Nanowires. *Nano Lett.* **2003**, *3*, 1745–1750.
- (25) Mooradian, A.; Wright, G. B. First Order Raman Effect in III–V Compounds. *Solid State Commun.* **1966**, *4*, 431–434.
- (26) Sahoo, P.; Tyagi, A. K.; Raj, B.; Dhara, S. Surface Optical Modes in Semiconductor Nanowires. In *Nanowires—Implementations and Applications*; Hashim, A. A., Ed.; IntechOpen: London, 2011.
- (27) Assali, S.; Greil, J.; Zardo, I.; Belabbes, A.; de Moor, M. W. A.; Koelling, S.; Koenraad, P. M.; Bechstedt, F.; Bakkers, E. P. A. M.; Haverkort, J. E. M. Optical Study of the Band Structure of Wurtzite GaP Nanowire. *J. Appl. Phys.* **2016**, *120*, 044304.
- (28) Bimberg, D.; Sondergeld, M.; Grobe, E. Thermal Dissociation of Excitons Bound to Neutral Acceptors in High-Purity GaAs. *Phys. Rev. B: Solid State* **1971**, *4*, 3451–3455.
- (29) Thomas, D. G.; Hopfield, J. J. Isoelectronic Traps Due to Nitrogen in Gallium Phosphide. *Phys. Rev.* **1966**, *150*, 680–689.
- (30) Baraban, A. P.; Samarin, S. N.; Prokofiev, V. A.; Dmitriev, V. A.; Selivanov, A. A.; Petrov, Y. Luminescence of SiO<sub>2</sub> Layers on Silicon at Various Types of Excitation. *J. Lumin.* **2019**, *205*, 102–108.
- (31) O'Donnell, K. P.; Chen, X. Temperature Dependence of Semiconductor Band Gaps. *Appl. Phys. Lett.* **1991**, *58*, 2924.
- (32) Smiri, B.; Saidi, F.; Mlayah, A.; Maaref, H. Power- and Temperature-Dependent Photoluminescence Investigation of Carrier Localization at Inverted Interface Transitions in InAlAs/InP Structures. *Jpn. J. Appl. Phys.* **2020**, *59*, 022001.
- (33) Maliakkal, C. B.; Gokhale, M.; Parmar, J.; Bapat, R. D.; Chalke, B. A.; Ghosh, S.; Bhattacharya, A. Growth, Structural and Optical Characterization of Wurtzite GaP Nanowires. *Nanotechnology* **2019**, *30*, 254002.
- (34) Halder, N. N.; Cohen, S.; Gershoni, D.; Ritter, D. Growth of Large Diameter Pure Phase Wurtzite GaP Nanowires by a Two-Step Axial-Radial Growth Approach. *Appl. Phys. Lett.* **2018**, *112*, 133107.

## Recommended by ACS

### Enhanced Optical Absorption of GaAs Near-Band-Edge Transitions in GaAs/AlGaAs Core-Shell Nanowires: Implications for Nanowire Solar Cells

Arrianna Creti, Mauro Lomascolo, *et al.*

DECEMBER 01, 2022

ACS APPLIED NANO MATERIALS

READ 

### Direct Band Gap AlGaAs Wurtzite Nanowires

Daniele Baretton, Nika Akopian, *et al.*

JANUARY 17, 2023

NANO LETTERS

READ 

### GaAs/GaAsSb Core-Shell Configured Nanowire-Based Avalanche Photodiodes up to 1.3 μm Light Detection

Rabin Pokharel, S. Iyer, *et al.*

MARCH 20, 2023

ACS APPLIED NANO MATERIALS

READ 

### Gallium Selenide Nanoribbons on Silicon Substrates for Photodetection

Pauline Hauchecorne, Thierry Baron, *et al.*

JULY 21, 2021

ACS APPLIED NANO MATERIALS

READ 

Get More Suggestions >